International Journal of Adhesion & Adhesives 30 (2010) 636–642

Contents lists available at ScienceDirect

International Journal of Adhesion & Adhesives

journal homepage: www.elsevier.com/locate/ijadhadh

Elastic analysis of interfacial stresses for the design of a strengthened FRP plate bonded to an RC beam

Boucif Guenaneche [a], Baghdad Krour [a,b], Abdeloauhed Tounsi [a,c,*], Abdelkader Fekrar [a], Samir Benyoucef [a], El Abbas Adda Bedia [a]

[a] Laboratoire des Matériaux et Hydrologie, Université de Sidi Bel Abbes, BP 89 Cité Ben M'hidi, 22000 Sidi Bel Abbes, Algérie
[b] Universitaire Mustapha Stambouli, Mascara, Département de Génie Civil, Algérie
[c] Département de génie civil, Faculté des Sciences de l'Ingénieur, Université Sidi Bel Abbes, Algérie

ARTICLE INFO

Article history:
Accepted 5 June 2010
Available online 16 June 2010

Keywords:
RC beams
Composite plate
Interfacial stresses
Relative humidity
Creep
Shrinkage

ABSTRACT

In this paper, the problem of interfacial stresses in RC beams strengthened with bonded composite laminates is analyzed using linear elastic theory. It explicitly considers the interface slip effect on the structural performance by including both the effect of the adherend shear deformations and the time-dependent deformations (such as shrinkage and creep). This new method needs only one differential equation to determine both shear and normal interfacial stress whereas the others solutions need two differential equations. Closed-form solutions are derived for plated RC beams simply supported at both ends and verified through direct comparisons with existing results. A parametrical study is carried out to show the effects of some design variables, e.g., thickness of adhesive layer and FRP plate.

1. Introduction

Engineering of modern composite materials has had a significant impact on the technology of design and construction. The main objective of using or selecting any material in construction is to make use of its properties efficiently for best performance and durability of the structure. The merits of a material are based on factors such as availability, structural strength, durability, and workability. Advanced composite materials, e.g. fibre-reinforced polymers (FRP), have found new applications in the rehabilitation of reinforced concrete structures [1,2]. The transferring of stresses from concrete to the FRP reinforcement is central to the reinforcement effect of FRP-strengthened concrete structures. This is because these stresses are likely to cause undesirable premature and brittle failure. In strengthening reinforced concrete beams with FRP strips, different failure modes have been observed [3–8]. One of the important failure modes is the plate end debonding of the soffit plate from concrete beam, which depends largely on the interfacial shear and normal stress concentration at the cut-off points of the plate. Many studies have been conducted, either analytically, numerically or both, to predict interfacial stresses, see, for example, those by Vilnay [9], Roberts [10], Roberts and Haji-Kazemi [11], Taljsten [12], Malek et al. [13], Maalej and Bian [14], Teng and coworkers [15–18], Tounsi and Benyoucef [19], Cai et al. [20], and Benachour et al. [21].

Based on the solution of Tsai et al. [22], Tounsi [23] proposed a solution by incorporating effects of interface shear stress on deformation in adherends, which were ignored by Smith and Teng [15] when they uncoupled a coupled governing equation. Combining the shear deformable bi-beam theory with a linear elastic interface model, Wang [24] obtained the stress distribution and fracture along the interface. Recently, Tounsi et al. [25], and Qiao and Chen [26] provided an improved solution and a more accurate prediction compared to the above models.

In this study, an improved theory is developed to predict the interface stress distributions in a plated beam by including the shear-lag effect of adherends. It explicitly considers the interface slip effect on the structural performance. Comparatively to those of the cited methods above, the computed interfacial stresses are considerably smaller than those obtained by other models which neglect adherend shear deformations. Hence, the adopted improved model describes better actual response of FRP–RC hybrid beams and permits the evaluation of interfacial stresses, the knowledge of which is very important in the design of such structures. Another important issue in this study is the time-dependent analysis of interfacial stresses distribution in RC beams bonded with FRP plates. Indeed, in concrete structures, stresses and strains strongly depend on the rheological properties of concrete mainly creep and shrinkage. The adopted model

* Corresponding author at: Laboratoire des Matériaux et Hydrologie, Université de Sidi Bel Abbes, BP 89 Cité Ben M'hidi 22000 Sidi Bel Abbes, Algérie.
Tel.: +213 4854 9888.
E-mail address: tou_abdel@yahoo.com (A. Tounsi).

0143-7496/$ - see front matter © 2010 Elsevier Ltd. All rights reserved.
doi:10.1016/j.ijadhadh.2010.06.003

describes better the actual response of the FRP–RC hybrid beam and permits the evaluation of time-dependent interface stresses, the knowledge of which is very important in the design of such structures.

2. Analytical model for bonded repair considering interface slip

Consider a concrete beam (adherend 1) reinforced by a soffit plate (adherend 2) through a thin adhesive layer with the geometry parameters as shown in Fig. 1. As aforementioned, adherends are modelled as two Euler–Bernoulli (E–B) beams with the width of b_f and thickness of t_b and t_f, respectively, and they are bonded by an interface of thin adhesive layer with the width and thickness of b_f and t_a, respectively. Adherend 1 can be primarily made of conventional materials (e.g., reinforced concrete (RC) or wood material); while adherend 2 can be either a thin steel or FRP strengthening plate but not limited to these two types of materials. Three basic assumptions are made: (a) the shear stress in the interface is proportional to the shear slip; (b) the two bonded adherends have the same bending curvature at the same section; and (c) since the thickness of the adhesive is small, both the shear and peeling stresses in the adhesive are assumed constant across its thickness.

2.1. Shear stresses along the adhesively bonded interface

The assumption (a) results in

$$\tau(x) = k_{as} S(x) \tag{1}$$

where $S(x)$ is the shear slip in the interface between the two bonded adherends, $\tau(x)$ the interfacial shear stress, and k_{as} the shear stiffness of adhesive which is given by

$$k_{as} = \frac{G_a}{t_a} \tag{2}$$

where G_a is the shear modulus of adhesive.

The real deformed cross-section of each adherend is nonlinear, which deviates from the linear one assumed by Tsai et al. [22] and Tounsi [23]. Recently, Tounsi et al. [25] provided an improved solution and a more accurate prediction compared to the above models. In this respect, the present study expects to have higher accuracy and produces equivalent results as in high-order theories. Based on this recent work [25], the shear-lag effect of adherends is taken into account in assessing the shear slip $S(x)$, which is expressed as

$$S(x) = \left(u_f(x) - \frac{t_f}{2}\left(-\frac{dw_f(x)}{dx}\right)\right) - \left(u_b(x) + \frac{t_b}{2}\left(-\frac{dw_b(x)}{dx}\right)\right) - \left(\frac{t_b}{4G_b} + \frac{5t_f}{12G_f}\right)\tau(x) \tag{3}$$

where $u_i(x)$ and $w_i(x)$ are, respectively, the longitudinal middle plane displacements and the vertical displacements of beams (adherends) i ($i=b, f$), and G_i the shear modulus of adherend i.

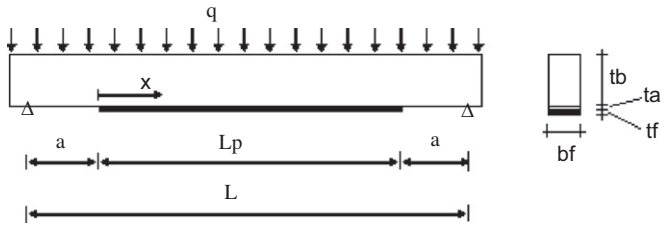

Fig. 1. Simply supported beam strengthened with bonded FRP plate.

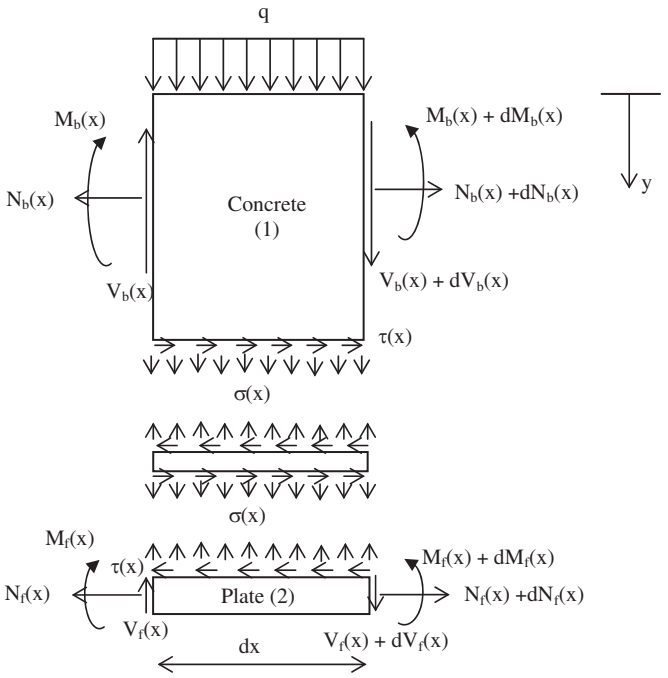

Fig. 2. Forces in infinitesimal element of a soffit-plated beam.

A typical infinitesimal isolated body of the plated beam is shown in Fig. 2, and the following equilibrium equations are established:

$$\frac{dN_b(x)}{dx} = -b_f\tau(x), \frac{dN_f(x)}{dx} = b_f\tau(x), \tag{4a}$$

$$\frac{dM_b(x)}{dx} = V_b(x) - b_f\frac{t_b}{2}\tau(x), \frac{dM_f(x)}{dx} = V_f(x) - b_f\frac{t_f}{2}\tau(x), \tag{4b}$$

$$\frac{dV_b(x)}{dx} = -r(x) - q, \frac{dV_f(x)}{dx} = r(x), \tag{4c}$$

$$V_b(x) + V_f(x) = V_T(x) \tag{4d}$$

where $N_b(x)$ and $N_f(x)$, $v_b(x)$ and $V_f(x)$, $M_b(x)$, and $M_f(x)$ are the internal axial forces, transverse shear forces, and bending moments in adherends 1 and 2, respectively, $v_T(x)$ the total applied transverse shear force, $\tau(x)$ the interface shear stress, and $r(x) = b_f\sigma(x)$ the normal force per unit length between adherend 1 and adherend 2 ($\sigma(x)$ is normal stress in the interface).

The assumed curvature compatibility between the two bodies gives the curvature ϕ as

$$\phi = \frac{M_b}{E_bI_b} = \frac{M_f}{E_fI_f} \tag{5}$$

where E_i and I_i are the Young's modulus and the moment of inertia of adherend "i" ($i=b, f$), respectively.

Solving Eqs. (4) and (5) yields

$$\frac{d\phi}{dx} = \frac{V_T - b_f d_c \tau(x)}{E_bI_b + E_fI_f} \tag{6}$$

where $d_c = (t_b + t_f)/2$.

According to the Euler–Bernoulli beam theory, the stresses and displacements of individual adherend can be related as

$$N_b(x) = E_bA_b\left(\frac{du_b(x)}{dx} - \alpha T_b\right), \quad N_f(x) = E_fA_f\frac{du_f(x)}{dx},$$
$$M_i(x) = -E_iI_i\frac{d^2w_i(x)}{dx^2} \tag{7}$$

where A_i is the cross-sectional area of adherend "i"($i=1, 2$). α, T_b, and αT_b are a linear coefficient of thermal expansion, the temperature distribution, and the shrinkage strain, respectively.

Differentiating Eq. (3) with respect to x once and combining with Eqs. (4), (6) and (7) yields

$$\frac{dS(x)}{dx}=\frac{N_f(x)}{E_fA_f}-\frac{N_b(x)}{E_bA_b}-\alpha T_b-d_c\phi(x)-\left(\frac{t_b}{4G_b}+\frac{5t_f}{12G_f}\right)\frac{d\tau(x)}{dx} \tag{8}$$

Using Eq. (1), the above equation becomes

$$\frac{dS(x)}{dx}=\gamma_s=\frac{K}{k_{as}}\left(\frac{N_f(x)}{E_fA_f}-\frac{N_b(x)}{E_bA_b}-\alpha T_b-d_c\phi(x)\right) \tag{9}$$

where γ_s is the shear slip strain and K is given by

$$K=\frac{1}{\left(\frac{1}{k_{as}}+\frac{t_b}{4G_b}+\frac{5t_f}{12G_f}\right)} \tag{10}$$

Taking a derivative with respect to x in Eq. (9) and then considering Eqs. (4a) and (6), the differential equation of slip displacement S is derived as

$$\frac{d^2S(x)}{dx^2}=\lambda^2S(x)-\theta V_T \tag{11}$$

$$\lambda^2=Kb_f\left[\frac{1}{E_bA_b}+\frac{1}{E_fA_f}+\frac{d_c^2}{E_bI_b+E_fI_f}\right] \tag{12}$$

$$\theta=\frac{K}{k_{as}}\frac{d_c}{E_bI_b+E_fI_f} \tag{13}$$

For simplicity, the general solutions presented below are limited to loading, which is either concentrated or uniformly distributed over part or the whole span of the beam, or both. For such loading, $d^2V_T(x)/dx^2=0$, and the general solution to Eq. (11) is given by

$$S(x)=B_1\cosh(\lambda x)+B_2\sinh(\lambda x)+m_1V_T(x) \tag{14}$$

where

$$m_1=\frac{\theta}{\lambda^2} \tag{15}$$

We note that in the above equations, $E_b=E_b(t)$ and $G_b=G_b(t)$ are the time-dependent tangent modulus of elasticity and the shear modulus of the concrete beam, respectively, given by Trost and Wolff [27]

$$E_b(t)=\frac{E_{bl}}{1+\chi\varphi(t,t_b)}\ \text{ and }\ G_b(t)=\frac{E_b(t)}{2(1+\upsilon)} \tag{16}$$

where E_{bl} is the tangent modulus of elasticity of the beam at time t_{bl}, χ an aging coefficient depending on strain development with time, and $t'_b=t_{bl}-t_{bc}$ (t_{bc} is the time of casting of beams and t_{bl} the time at initial loading of beams), $\varphi(t, t_b)$ the creep coefficient related to the elastic deformation at t'_b days, which is defined as [28]

$$\varphi(t,t_b)=\phi_{RH}\beta(f_{cm})\beta(t_b)\beta_{cb}(t-t_b) \tag{17}$$

where ϕ_{RH}, $\beta(f_{cm})$, and $\beta(t_b)$ are factors depending on the relative humidity, the concrete strength, and the concrete age loading, respectively, which are defined as

$$\phi_{RH}=1+\frac{1-\frac{RH}{100}}{0.10\sqrt[3]{h_0}} \tag{18}$$

$$\beta(f_{cm})=\frac{16.8}{\sqrt{f_{cm}}} \tag{19}$$

$$\beta(t_b)=\frac{1}{0.1+t'^{0.20}_b} \tag{20}$$

where RH is the relative humidity of the ambient environment in %, $h_0=2A_b/p_b$ is the notional size of the beam in mm, A_b the area of the beam cross section, p_b the beam perimeter in contact with the atmosphere, and f_{cm} the mean compressive strength of concrete in N/mm^2 at the age 28 days. Moreover, $\beta_{cb}(t-t'_b)$ in Eq. (17) is a coefficient for the development of creep with time, which is estimated from

$$\beta_{cb}(t-t_b)=\left(\frac{t-t'_b}{\beta_H+t-t'_b}\right)^{0.3} \tag{21}$$

where β_H is a coefficient depending on the relative humidity RH, given as

$$\beta_H=1.5(1+(0.012RH)^{18})h_0+250\le 1500 \tag{22}$$

The temperature T_b in Eq. (7) is given by

$$T_b=\frac{\varepsilon_{sb}(t-t_{bc})}{\alpha} \tag{23}$$

where $\varepsilon_{sb}(t-t_{bc})$, the shrinkage strain is calculated from

$$\varepsilon_{sb}(t-t_{bc})=\varepsilon_{sb}(f_{cm})\beta_{RH}\beta_{sb}(t-t_{bc}) \tag{24}$$

where $\varepsilon_{sb}(f_{cm})$, β_{RH} are factors depending on the concrete strength and the relative humidity, respectively, which are defined as

$$\varepsilon_{sb}(f_{cm})=[160+\beta_{sc}(90-f_{cm})]10^{-6} \tag{25}$$

$$\beta_{RH}=\begin{cases}-1.55(1-(RH/100)^3), \text{ for } 40\%\le RH\le 99\% \text{(stored in air)}\\ +0.25(1-(RH/100)^3), \text{ for } RH\ge 99\% \text{(immersed in water)}\end{cases} \tag{26}$$

where β_{sc} is a coefficient depending on the type of cement. Moreover, $\beta_{sb}(t-t_{bc})$ in Eq. (24) is a coefficient for the development of shrinkage with time, which is estimated from

$$\beta_{sb}(t-t_{bc})\left[\frac{t-t_{bc}}{0.035h_0^2+t-t_{bc}}\right]^{0.5} \tag{27}$$

Having derived the general solutions for the slip displacement S (Eq. (14)), B_1 and B_2 are constant coefficients determined from the boundary conditions. In the present study, a simply supported beam is investigated which is subjected to a uniformly distributed load. By substituting the expression for the shear force in a simply supported beam subjected to a uniformly distributed load into Eq. (14), the general solution for the slip displacement for this load case can be found as

$$S(x)=B_1\cosh(\lambda x)+B_2\sinh(\lambda x)+m_1q\left(\frac{L}{2}-x-a\right) \tag{28}$$

where q is the uniformly distributed load and x, a, L, and L_p are defined in Fig. 1. The constants of integration need to be determined by applying suitable boundary conditions. Considering the boundary conditions:

(1) Due to symmetry, the slip displacement S at mid-span is zero, i.e.

$$S\left(\frac{L_P}{2}\right)=B_1\cosh\left(\lambda\frac{L_P}{2}\right)+B_2\sinh\left(\lambda\frac{L_P}{2}\right)+m_1V_T\left(\frac{L_P}{2}\right)=0 \tag{29}$$

(2) At the end of the FRP plate, the longitudinal force $[N_b(0)=N_f(0)]$ and the moment $M_f(0)$ are zero. As a result, the moment in the section at the plate curtailment is resisted by the beam alone and can be expressed as

$$M_b(0)=\frac{qa}{2}(L-a) \tag{30}$$

Applying the above boundary condition in Eq. (9)

$$\gamma(x=0)=-m_2M_b(0)\ \text{ avec }\ m_2=\frac{K}{k_{as}}\left(\frac{d_c}{E_bI_b}+\frac{\alpha T_b}{M_b(0)}\right) \tag{31}$$

From the above three equations,

$$B_2 = \frac{-m_2 qa}{2\lambda}(L-a) + \frac{m_1}{\lambda}q \tag{32}$$

$$B_1 = -B_2 \tanh\left(\frac{\lambda L_p}{2}\right) \tag{33}$$

For practical cases $\lambda L_p/2 > 10$and as a result $\tanh(\lambda L_p/2) \approx 1$. So the expression for B_1 can be simplified to

$$B_1 = -B_2 \tag{34}$$

Substitution of B_1 and B_2 into Eq. (14) gives an expression for the interfacial shear stress at any point

$$S(x) = \left(\frac{m_2 a}{2}(L-a) - m_1\right)\frac{qe^{-\lambda x}}{\lambda} + m_1 q\left(\frac{L}{2} - a - x\right) \quad 0 \le x \le L_p \tag{35}$$

Using Eq. (1), the interfacial shear stress is given by

$$\tau(x) = k_{as} S(x) \tag{36}$$

2.2. Normal stresses along the adhesively bonded interface

The normal force $r(x)$ in the interface is regarded as a distributed load for adherend 2 and can thus be calculated considering Eqs. (4–6) as

$$r(x) = k_{as} b_f \left[\frac{t_f}{2} - d_c \frac{E_f I_f}{E_b I_b + E_f I_f}\right]\gamma_s(x) \tag{37}$$

Physically, both the shear force and the bending moment at the end of adherend 2 (free-end of the bonded plate) should be zero. However, since the shear interface stress τ is not zero at this point, the boundary condition of $V_f=0$ at this point cannot be fulfilled. In addition, for adherend 2 to maintain the same curvature as adherend 1, $M_f=0$ at this free-end cannot be satisfied either. To correct this boundary condition, these non-zero values can be calculated and equal and opposite forces can be applied to the ends of FRP plate. The vertical force at the end of FRP plate can be derived by equilibrium

$$V_f(0) = \frac{E_f I_f}{E_b I_b + E_f I_f} V_T + k_{as} b_f \left[\frac{t_f}{2} - d_c \frac{E_f I_f}{E_b I_b + E_f I_f}\right] S(0) \tag{38}$$

From Eq. (5), the non-zero moment of FRP plate at the end of plate is calculated as

$$M_f(0) = \frac{E_f I_f}{E_b I_b} M_b(0) \tag{39}$$

The shear force in Eq. (38) and the moment in Eq. (39) are applied back to the ends of FRP plate to correct the incompatible boundary conditions. Assume that the section dimensions of concrete beam are much larger than those of FRP plate (such as in the case of beams repaired with thin plates) and these correction forces are relatively small, the deformation of concrete beam due to these correction forces is then negligible and assumed to be rigid in this calculation. The calculation model will then be reduced to a beam (FRP plate) on an elastic foundation (adhesive) with vertical spring stiffness k_{an}. Using the theory of a beam on an elastic foundation, we have the vertical displacement of FRP plate as

$$w = \frac{e^{-\chi}}{k_{an}}\left[2\beta_s V_b(0)\cos(\chi) - 2\beta_s^2 M_b(0)(\cos(\chi) - \sin(\chi))\right] \tag{40}$$

where

$$\chi = \beta_s x \tag{41}$$

$$\beta_s = \left(\frac{k_{an}}{4E_f I_f}\right)^{1/4} \tag{42}$$

$$k_{an} = \frac{E_a b_f}{t_a} \tag{43}$$

where E_a is the elastic modulus of adhesive.

The total normal stress σ in the interface (from both the external vertical force and the boundary correction forces) is derived as

$$\sigma(x) = \frac{r + k_{an} w}{b_f}. \tag{44}$$

3. Results and discussions

An RC beam bonded with a CFRP soffit plate is being considered. The beam is simply supported and subjected to a uniformly distributed load. The span of The RC beam is 3000 mm, the distance from the support to the end of the plate is 300 mm, and the uniformly distributed load $q=50$ KN/m.

On the basis of the presented analytical method, a computer program has been written.

3.1. Comparisons with existing models

As a verification of the present solution, comparisons of the present model with typical existing analytical solutions [15, 23, and 25] are made without the shrinkage and creep effect. As an example, a reinforced concrete (RC) beam strengthened by a CFRP plate studied by Smith and Teng [15], Tounsi [23], and Tounsi et al. [25] is investigated.

The results of the peak interface stresses at the plate end for the two load cases are summarized in Table 1. The solutions of the peak interface shear stress at the plate end by Smith and Teng [15] are larger than the one from the present solution; while the one by Tounsi [23] is smaller compared to the present prediction. Our results agree reasonably well with those reported by Tounsi et al. [25].

The interface stress distributions obtained by the present study and the solution presented by Tounsi et al. [25] are shown in Fig. 3 for an RC beam bonded with CFRP plate under uniformly distributed load (UDL). It is apparent that the agreement is good.

3.2. Theoretical parametric study

In this section, numerical results of the present solutions are presented to study the effect of various parameters on the time development of the edge interfacial stresses. The influence of creep and shrinkage on edge interfacial stresses is taken into account. These results are intended to demonstrate the main characteristics of edge interfacial stress in these strengthened beams.

The following data have been used for the following numerical results: concrete *C*25/30, $f_{cm}=25$ MPa, $RH=40\%$, $t_b=28$ days, $E_{bl}=E_{c28}=30$ GPa and $\beta_{SC}=5$ (normal or rapid hardening cement). The width and the depth of the RC beam are, 200 and 300 mm, respectively. The geometric and material properties of both CFRP bonded plate and the adhesive layer, are given in Table 2.

Table 1
Comparison of peak interface shear and normal stresses.

Theory	τ (MPa)	σ (MPa)
Smith and Teng [15]	2.740	1.484
Tounsi [23]	1.474	0.861
Tounsi et al. [25]	1.602	0.928
Present model	1.603	0.859

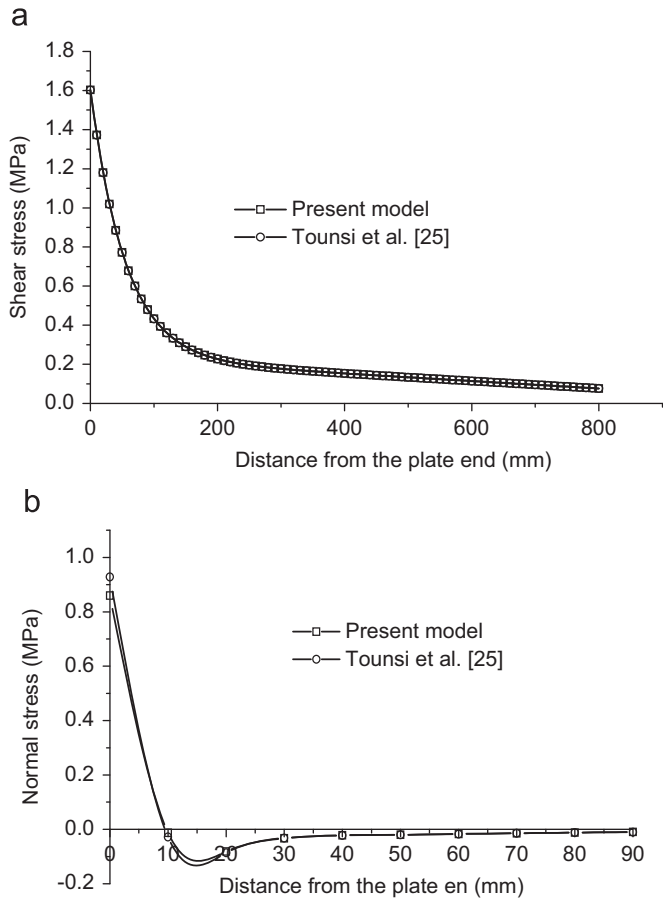

Fig. 3. Comparison of interface stresses in the CFRP-strengthened RC beam under uniformly distributed load (UDL): (a) shear stress and (b) normal stress.

Table 2
Geometric and material properties.

Material	E (GPa)	G (GPa)	υ	Width (mm)	Depth (mm)
CFRP plate $[0_{16}]_S$	140	5	0.28	b_f=200	$t_{f=}$4
Adhesive layer	3		0.35	b_f=200	t_a=2

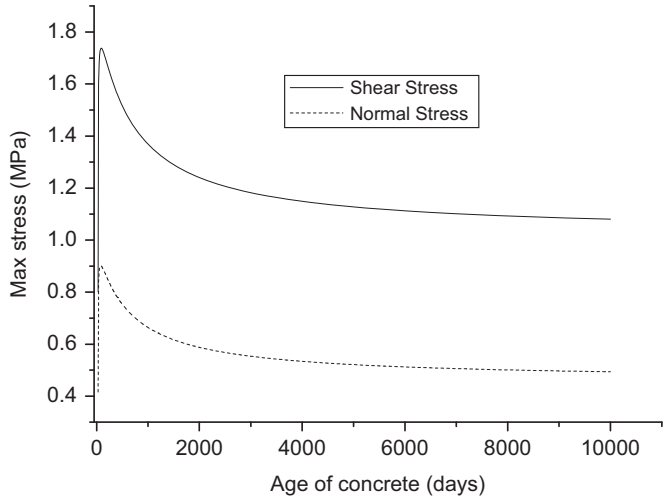

Fig. 4. Time development of interfacial edge stresses for an RC beam with a bonded CFRP soffit plate $[0_{16}]_S$.

In Fig. 4 the time development of the edge interfacial stresses is presented. From the obtained results we can conclude that the edge interfacial stresses exhibit the lower value at 28 days. After this time, these stresses take peak value during the first months and begin to decrease until they become almost constant at very large time.

Peak shear and peeling stresses for various thicknesses of the FRP plate appear in Figs. 5 and 6, respectively. The results reveal that thickness of the FRP plates significantly increases the edge peeling and shear stresses. This relation is an outcome of the local bending effects in the FRP plate governed by the flexural rigidity of the plate. Thus any increase in the flexural rigidity leads to an increase in the magnitude of the edge stresses.

Figs. 7 and 8 show the effects of the thickness of the adhesive layer on the time development of interfacial edge stresses. The interfacial edge stresses increase as the thickness of FRP plate decreases. However, design of properties and thickness of the adhesive is a difficult problem. An optimization design of the adhesive is expected.

The numerical results in Figs. 9 and 10 show that the property of the adhesive hardly influences the level of the interfacial edge stresses. The stress concentrations at the end of the plate increase as the Young's modulus of the adhesive increases.

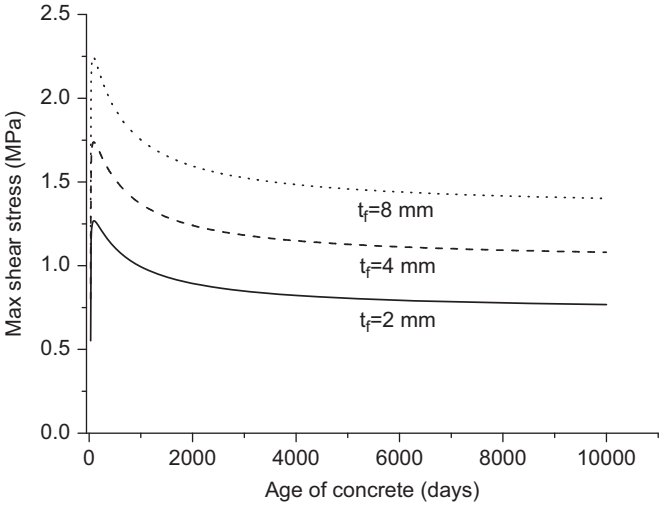

Fig. 5. Effect of FRP thickness on time development of interfacial edge shear stresses for an RC beam with a bonded CFRP soffit plate (q=50 kN/m).

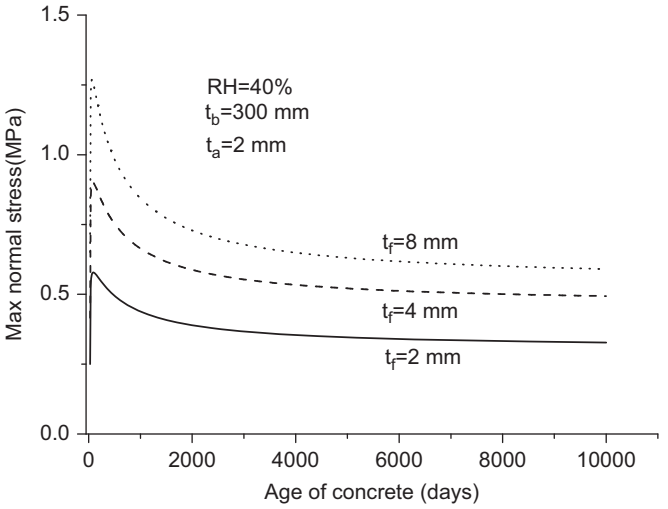

Fig. 6. Effect of FRP thickness on time development of interfacial edge normal stresses for an RC beam with a bonded CFRP soffit plate (q=50 kN/m).

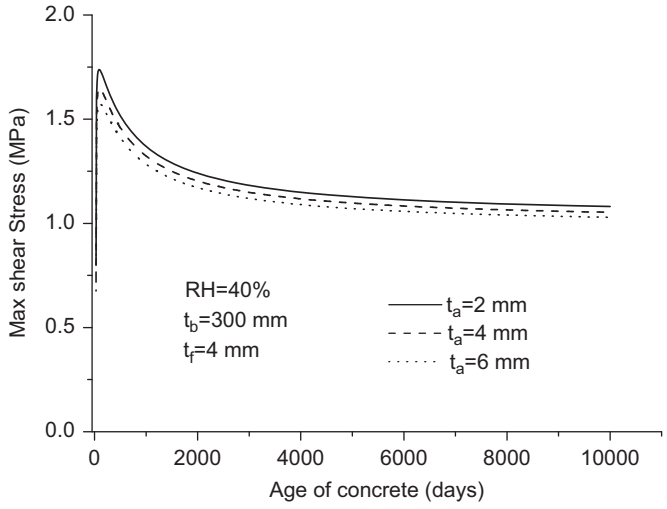

Fig. 7. Effect of the adhesive thickness on time development of interfacial edge shear stresses for an RC beam with a bonded CFRP soffit plate (q=50 kN/m).

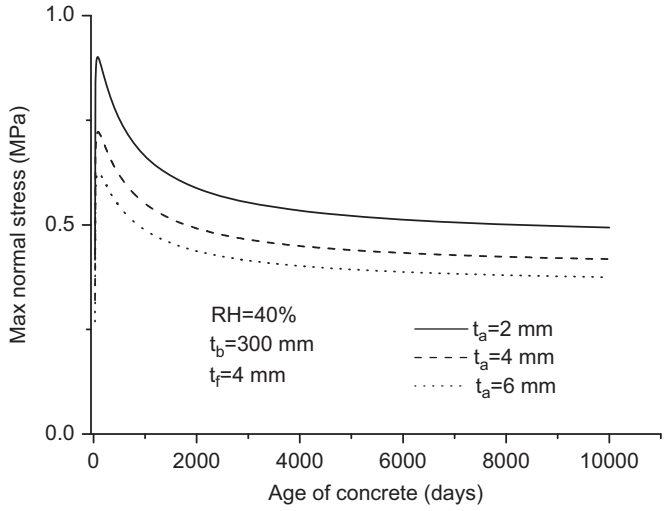

Fig. 8. Effect of the adhesive thickness on time development of interfacial edge normal stresses for an RC beam with a bonded CFRP soffit plate (q=50 kN/m).

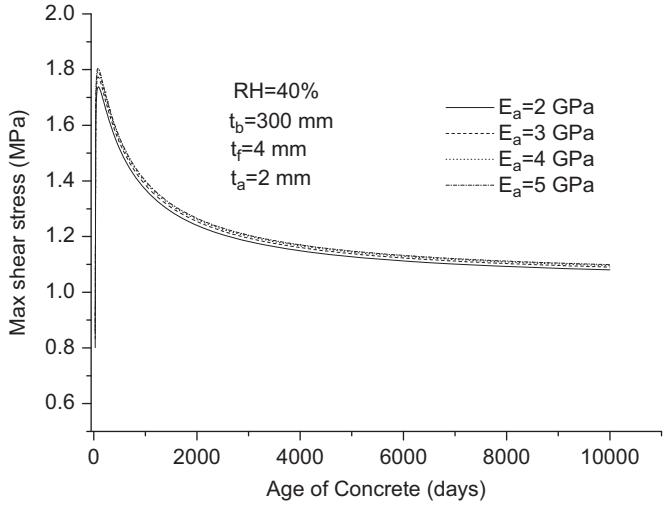

Fig. 9. Effects of adhesive moduli on time development of interfacial edge shear stresses for an RC beam with a bonded CFRP soffit plate (q=50 kN/m).

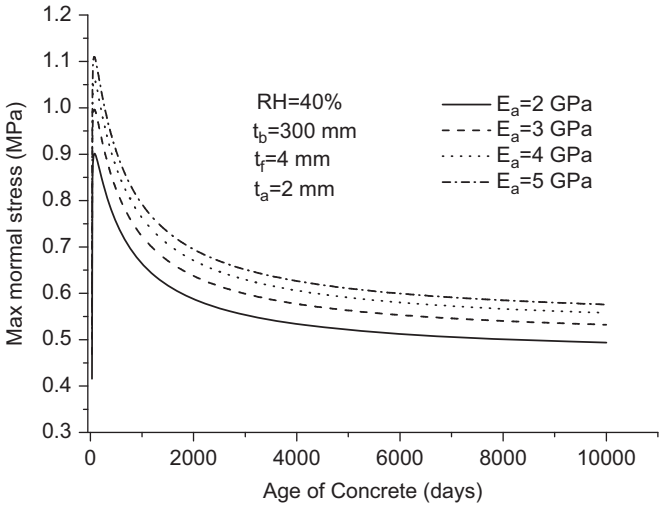

Fig. 10. Effects of adhesive moduli on time development of interfacial edge normal stresses for an RC beam with a bonded CFRP soffit plate (q=50 kN/m).

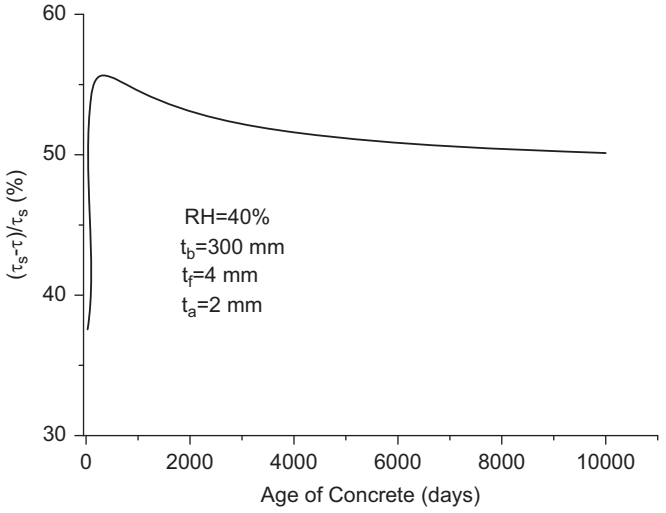

Fig. 11. Solution difference percentage for interfacial edge shear stresses for an RC beam with a bonded CFRP soffit plate (q=50 kN/m).

To supply information on the contribution of adherend shear deformations to interfacial stresses, the relative difference between the edge interfacial stress solutions (σ, τ) and (σ_s, τ_s) is examined. σ_s and τ_s are normal stress and shear stress in the interface between the two bonded adherends, respectively, with neglecting adherend shear deformations effect. It is obvious that a greater solution difference percentage implies a more important adherend shear deformations effect on the interfacial stresses.

In Figs. 11 and 12, the solution difference percentage of the edge interfacial stresses during time is presented. From the obtained results we can conclude that the adherend shear deformations effect is less important at 28 days. After this time, this effect becomes very significant during the first months and begins to decrease until they become almost constant at very large time.

4. Concluding remarks

The present study has developed a relatively simple procedure for predicting the performance of two bonded solid bodies using a simple beam theory and equilibrium conditions while considering explicitly the interface slip, the adherend shear deformations and

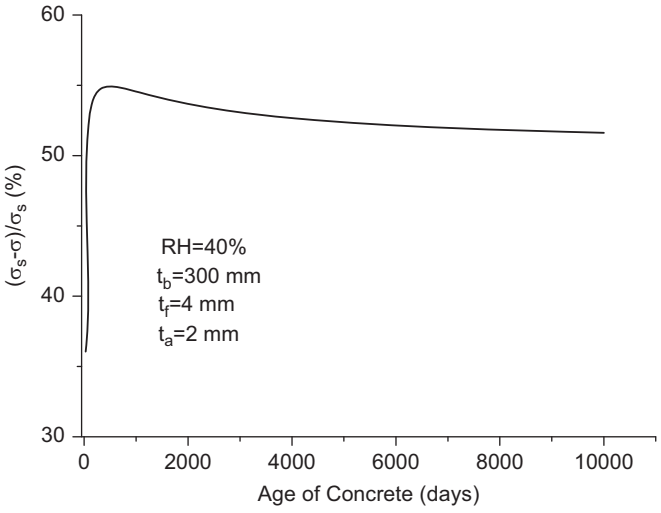

Fig. 12. Solution difference percentage for interfacial edge normal stresses for an RC beam with a bonded CFRP soffit plate (q=50 kN/m).

the rheological properties of concrete mainly creep and shrinkage. The solutions were then modified to satisfy the boundary conditions by applying derived correction forces back to the ends of the repairing plate through a beam-on-elastic-foundation approach. The present study showed that interfacial stresses take a peak value during the first months and begin to decrease until they become almost constant after a very long time. In addition, interfacial stresses are influenced by geometry parameters such as thickness of the FRP plate and adhesive layer in the range of different degrees. The solutions can be used as benchmark for other numerical methods and also the experimental results.

References

[1] Triantafillou TC. Composites: a new possibility for the shear strengthening of concrete, masonry and wood. Compos Sci Technol 1998;58:1285–95.
[2] Quantrill RJ, Hollaway LC. The flexural rehabilitation of reinforced concrete beams by the use of prestressed advanced composite plates. Compos Sci Technol 1998;58:1259–75.
[3] Gao B, Leung CKY, Kim JK. Failure diagrams of FRP strengthened RC beams. Compos Struct 2007;77:493–508.
[4] Diab H, Wu Z. Nonlinear constitutive model for time-dependent behavior of FRP–concrete interface. Compos Sci Technol 2007;67:2323–33.
[5] Pan J, Leung CKY. Debonding along the FRP–concrete interface under combined pulling/peeling effects. Eng Fract Mech 2007;74:132–50.
[6] Gao B, Leung CKY, Kim JK. Prediction of concrete cover separation failure for RC beams strengthened with CFRP strips. Eng Struct 2005;27:177–89.
[7] Lau KT, Zhou LM, Wu JS. Investigation on strengthening and strain sensing technique for concrete structure. J Mater Struct 2001;34:42–50.
[8] Buyukozturk O, Hearing B. Failure behaviour of precracked concrete beams retrofitted with FRP. J Compos Constr 1998;2:138–44.
[9] Vilnay O. The analysis of reinforced concrete beams strengthened by epoxy bonded steel plates. Int J Cem Compos Lightweight Concr 1988;10(2): 73–78.
[10] Roberts TM. Approximate analysis of shear and normal stress concentrations in the adhesive layer of plated RC beams. Struct Eng 1989;67(12): 229–233.
[11] Roberts TM, Haji-Kazemi H. Theoretical study of the behavior of reinforced concrete beams strengthened by externally bonded steel plates. Proc Inst Civ Eng 1989;87(Part 2):39–55.
[12] Taljsten B. Strengthening of beams by plate bonding. J Mater Civ Eng—ASCE 1997;9(4):206–212.
[13] Malek AM, Saadatmanesh H, Ehsani MR. Prediction of failure load of R/C beams strengthened with FRP plate due to stress concentration at the plate end. ACI Struct J 1998;95(1):142–152.
[14] Maalej M, Bian Y. Interfacial shear stress concentration in FRP strengthened beams. Compos Struct 2001;54(4):417–426.
[15] Smith ST, Teng JG. Interfacial stresses in plated beams. Eng Struct 2001;23(7): 857–871.
[16] Shen HS, Teng JG, Yang J. Interfacial stresses in beams and slabs bonded with thin plate. J Eng Mech—ASCE 2001;127(4):399–406.
[17] Teng JG, Zhang JW, Smith ST. Interfacial stresses in reinforced concrete beams bonded with a soffit plate: a finite element study. Constr Build Mater 2002;16(1):1–14.
[18] Teng JG, Cheng JF, Smith ST, Lam L. Behavior and strength of FRP-strengthened RC structures: a state-of-the-art review. Proc Inst Civ Eng—Struct Build 2003;156(1):51–62.
[19] Tounsi A, Benyoucef S. Interfacial stresses in externally FRP plated concrete beams. Int Adhes Adhes 2007;27:207–15.
[20] Cai CS, Nie J, Shi XM. Interface slip effect on bonded plate repairs of concrete beams. Eng Struct 2007;29:1084–95.
[21] Benachour A, Benyoucef S, Tounsi A. Adda bedia E.A. Interfacial stress analysis of steel beams reinforced with bonded prestressed FRP plate. Eng Struct 2008;30:3305–15.
[22] Tsai MY, Oplinger DW, Morton J. Improved theoretical solutions for adhesive lap joints. Int J Solids Struct 1998;35(12):1163–1185.
[23] Tounsi A. Improved theoretical solution for interfacial stresses in concrete beams strengthened with FRP plate. Int J Solids Struct 2006;43:4154–4174.
[24] Wang JL. Mechanics and fracture of hybrid material interface bond. PhD dissertation, Akron (OH, USA), Department of Civil Engineering, The University of Akron, 2003.
[25] Tounsi A, Hassaine Daouadji T, Benyoucef S, Adda bedia EA. Interfacial stresses in FRP-plated RC beams: effect of adherend shear deformations. Int J Adhes Adhes 2009;29:343–51.
[26] Qiao P, Chen F. An improved adhesively bonded bi-material beam model for plated beams. Eng Struct 2008;30(7):1949–57.
[27] Trost H, Wolff J. Zur wirklichkeitsnahen ermittlung der beanspruchungen in abschnittsweise hergestellten spannbetontragwerken. Bauingenieur 1970;45: 155–69.
[28] Eurocode 2 Editorial Group. Design of concrete structures, part 1: General rules and rules for buildings. Eurocode no. 2, Brussels, 1991.